Cytosolic Region of TM6 in P-Glycoprotein: Topographical Analysis and Functional Perturbation by Site Directed Labeling[†]

Janet Storm,[‡] Szabolcs Modok,[‡] Megan L. O'Mara,[§] D. Peter Tieleman,[§] Ian D. Kerr,[△] and Richard Callaghan*[,‡]

Nuffield Department of Clinical Laboratory Sciences, John Radcliffe Hospital, University of Oxford, United Kingdom, Department of Biological Sciences, University of Calgary, 2500 University Drive NW, Calgary, Alberta T2N 1N4, Canada, and Centre for Biochemistry and Cell Biology, School of Biomedical Sciences, University of Nottingham, United Kingdom

Received November 22, 2007; Revised Manuscript Received January 30, 2008

ABSTRACT: Reduced intracellular drug accumulation due to the activity of the drug efflux pump ABC^{B1} is a major mechanism in the resistance of cancer cells to chemotherapy. ABC^{B1} is a poly specific transporter, and the molecular mechanism of its complex translocation process remains to be elucidated. To understand the process will require information on the regions involved in drug binding and those that couple this event to nucleotide hydrolysis. The present investigation focuses on the cytosolic region of transmembrane helix 6 (TM6), which has been widely attributed with a central role in the translocation process. A series of ABC^{B1} isoforms containing a unique cysteine within TM6 was constructed and the resultant proteins purified and reconstituted. Accessibility of the cysteines to covalent modification by maleimide reagents was measured for the basal, ATP bound and vanadate trapped conformations of each isoform. Residues at the two extremes of the TM6 region examined (amino acids 344 to 360) were considerably more accessible than the central segment, the latter of which also failed to undergo significant conformational changes during the catalytic cycle. Covalent modification of the cytosolic segment of TM6 did, however, attenuate drug stimulation of ATP hydrolysis and demonstrates an important role for this segment in coupling drug binding to ATP hydrolysis during translocation.

Cancer cells either inherently display or develop a resistance to the majority of anticancer drugs used in the clinic. The resistant phenotype is borne of a number of cellular and multicellular mechanisms, and the presence of drug efflux pumps on the cell surface provides a first line of defense (*1*). The efflux pumps associated with cancer resistance belong to the ATP binding cassette (ABC[1]) family of transporters (*1–3*) and display an ability to interact with an incredibly large number of pharmacological agents. In fact, the ABC^{B1} (P-glycoprotein) transporter is known to interact with over 200 drugs, a feature that has been described as poly specificity (*4*). Two other members (ABC^{C1} and ABC^{G2}) make up the triumvirate of multidrug efflux pumps, and despite their poly specificity, the transporters display only a low degree of substrate overlap. Each of the transporters generates the poly specificity through the provision of multiple pharmacologically distinct sites for drug interaction (*5–7*). The complex nature of drug–protein interactions for multidrug efflux pumps has been a contributing factor to the lack of development of specific inhibitors capable of overcoming their actions.

The most intensively studied multidrug transporter is ABC^{B1}, and this protein has been shown to display a minimum of four distinct drug binding sites, which are allosterically linked to each other (*8–11*). However, drug binding represents only an initial step in the overall drug translocation process, which shows additional allostery between the drug binding sites and the NBDs, coupling nucleotide hydrolysis in order to maintain an active process. ABC^{B1} contains two NBDs, each of which is both essential for drug transport and capable of mediating ATP hydrolysis (*12–15*). However, there is controversy regarding the stoichiometry of coupling and whether both NBDs are involved in each translocation event (*16–21*). There is considerable evidence for a two-way communication between the NBDs and the drug binding sites within the transmembrane domains (TMDs). For example, a number of transported substrates and inhibitors of ABC^{B1} are able to modulate the maximal rate of ATP hydrolysis (*22–24*). Similarly, the binding of ATP analogues, or trapping the protein with ADP and vanadate, causes considerable conformational changes within the TMD as demonstrated through low resolution structural analyses (*25–27*). These conformational changes impact on the translocation process by varying substrate binding site conformations between a high affinity inward facing to a

[†] This investigation was generously supported by a Cancer Research UK Program Grant (C362/A913) for which R.C. was the principal investigator. Modeling studies were supported by the Canadian Institutes of Health Research and Alberta Heritage Foundation for Medical Research.

* Corresponding author. Dr Richard Callaghan, Nuffield Department of Clinical Laboratory Sciences, Level 4, John Radcliffe Hospital, University of Oxford, Oxford UK, OX3 9DU. Tel: +44 1865 221 110. Fax: +44 1865 221 834. E-mail richard.callaghan@ndcls.ox.ac.uk.

[‡] University of Oxford.

[§] University of Calgary.

[△] University of Nottingham.

[1] Abbreviations: ABC, ATP binding cassette; ABCB1, P-glycoprotein; NBD, nucleotide binding domain; TMD, transmembrane domain; TM6, transmembrane helix 6; [^{125}I]-IAAP, [^{125}I]-iodoaryl-azido-prazosin; ANOVA, analysis of variance; CM, coumarin maleimide; FM, fluorescein maleimide; BM, BODIPY maleimide; MTS, methano-thiosulfonate.

10.1021/bi7023089 CCC: $40.75
Published on Web 02/28/2008

low affinity outward facing orientation (*28*). Yet many unanswered questions remain regarding the mechanism of drug translocation by ABC^{B1}, including (i) the location of the drug binding sites, (ii) regions involved in coupling to the NBDs, and (iii) whether coupling is funneled through a single pathway common to all transported drugs, or through several routes specific to each binding site.

Numerous attempts have been made to elucidate which transmembrane helices are involved in the translocation process, in particular those contributing to the drug binding site(s). Approaches have involved the use of photoactivatable drug analogues, naturally occurring mutant isoforms, directed mutagenesis, and cysteine scanning mutagenesis (*29–36*). Perturbation of transmembrane helix six (TM6) was commonly employed, and this segment has been widely implicated in mediating drug binding or contributing in some manner to the translocation pathway (*37–41*). Previous investigations from our laboratories focused on the extracellular half-of TM6 (TM6$_{EXT}$) to generate topography for the helix and to describe the functional roles of residues along it (*42, 43*). The residues along this segment of the helix (i.e., 331 to 343) were assessed for accessibility to covalent modification and the topography interpreted using an initial homology model for ABC^{B1}. Moreover, TM6$_{EXT}$ was not involved in drug binding *per se*, but was able to influence the basal (i.e., drug free) rate of ATP hydrolysis, thereby indicating an important role in the translocation process. In addition, TM6$_{EXT}$ underwent considerable alteration when ABC^{B1} was switched between conformations dictated by the ATP hydrolytic process and the nature of the change was suggested as a helical tilting (*42*).

Clearly, TM6 plays a crucial role in the drug translocation mechanism of ABCB1 and the present investigation focuses on residues in the cytoplasmic half of the helix (TM6$_{CYT}$) and in the helical extension, or intracellular domain, linking TM6 to the N-terminal NBD. The topography of this region is described for the basal, nucleotide bound, and vanadate trapped conformations of ABC^{B1} to fully ascertain the role of this key helix in the overall multidrug translocation mechanism.

MATERIALS AND METHODS

Materials. Coumarin- (CM), fluorescein- (FM), and BODIPY-maleimide (BM) were purchased from Molecular Probes (Leiden, NL). The Ni-NTA His-Bind Superflow resin and octyl-β-D-glucoside were obtained from Merck Biosciences (Nottingham, UK). Insect X-press and Excell 405 insect cell tissue culture media were purchased from Cambrex BioScience (Nottingham, UK) and AMS Biotechnology (Abingdon, UK), respectively. Vinblastine sulfate, nicardipine hydrochloride, cholesterol, adenosine triphosphate magnesium salt, adenosine 5′-(β,γ-imido)triphosphate tetralithium salt hydrate (AMP-PNP), and sodium orthovanadate were all obtained from Sigma (Poole, UK). Crude *Escherichia coli* lipid extract was purchased from Avanti Polar Lipids (Alabaster, USA). [^{125}I]-Iodoarylazidoprazosin (81.4 TBq/mmol) was obtained from Perkin-Elmer LAS (Beaconsfield, UK).

Cell Culture. Single cysteine containing mutant isoforms of ABC^{B1} (S344C, V345C, G346C, Q347C, S349C, A354C, and G360C) were constructed as previously described (*44*) using site directed mutagenesis with the Altered Sites II (Promega) or the QuickChange (Stratagene) systems. All mutagenesis employed the cysteine-less protein as a template, which bears a C-terminal hexahistidine tag (*24*). The cDNA for each isoform was used to generate recombinant baculovirus in the Sf9 insect cell line (*24*). Trichplusia ni (High-5) insect cells grown as shaking cultures were infected with the final high titer, purified recombinant baculovirus at a multiplicity of infection of 5–10, for a period of 72 h (for optimal ABC^{B1} expression (*24*)) prior to harvesting by centrifugation (2000*g*, 10 min).

Protein Production. Crude membrane fractions were obtained from the infected High-5 cells using four rounds of nitrogen cavitation (20 min, 4 °C, and 1500 p.s.i N_2) and sucrose density ultracentrifugation (100,000*g* 60 min) as previously described (*24*). The harvested crude membranes were immediately frozen and stored at −80 °C for up to six months. ABC^{B1} was solubilized from the membranes with 2% (w/v) octyl-β-D-glucoside in the presence of 0.4% (w/v) crude lipids (4:1 *E. coli* lipids:cholesterol) and purified with immobilized metal affinity chromatography. The chromatography with Ni-NTA His-Bind resin was achieved using a gravity flow system as previously described (*24*). Elution of the protein was achieved with a step gradient of imidazole (5–250 mM) and the purified ABC^{B1} immediately reconstituted into *E. coli* lipids:cholesterol vesicles by specific adsorption of detergent onto SM-2 BioBeads. Successful reconstitution of ABC^{B1} was routinely assessed with relative migration of lipids and proteins through a discontinuous sucrose density gradient (*24*). Purified, reconstituted ABC^{B1} was used immediately or snap frozen and stored at −80 °C with a less than 15% drop in activity over a 15-month period.

ATPase Activity. The ATPase activity of all ABC^{B1} isoforms was determined using an adaptation (*24*) of the colorimetric assay described by Chifflet et al. (*45*) to measure inorganic phosphate liberation. Proteoliposomes (0.2–0.5μg) were incubated with varying ATP concentrations (0–2 mM) in the presence or absence of drug substrate (30 μM vinblastine) or modulator (10 μM nicardipine) as previously detailed (*42*). This assay was used to determine the affinity constant for ATP (K_M) and the maximal enzyme activity (V_{max}) by Michaelis–Menten analysis under basal (drug free) or drug stimulated conditions. The parameters were obtained by nonlinear least-squares regression of the following equation: $V = (V_{max} \cdot [S])/(K_M + [S])$, where [S] is the concentration of ATP.

The second type of assay was used to characterize drug interaction with the protein to ascertain the potency (EC_{50}) and degree to which ATPase activity could be stimulated. Proteoliposomes (0.2–0.5 μg) were incubated with a constant ATP concentration (1.75 mM) and varying drug concentrations (10^{-9} to 10^{-4} M) as previously described (*42*). The activity was plotted as a function of drug concentration and the drug potency ascertained by nonlinear regression of the general dose−response equation: $v = V_{min} + (V_{max} - V_{min})/(1 + 10^{\log EC_{50} - [S]})$, where V_{min} is the minimal ATPase activity, V_{max} is the maximal activity, and [S] is the ATP concentration.

Cysteine Labeling of Mutant ABC^{B1} Isoforms. The mutant ABC^{B1} isoforms were reacted with maleimide probes to ascertain the accessibility of the introduced cysteine residues. Three thiol-reactive fluorescent maleimide probes with distinct physicochemical properties were used: fluorescein−

maleimide (hydrophilic), courmarin−maleimide (hydrophobic), and BODIPY−maleimide (zwitterionic). The procedure has been described in more detail previously (*42*). Briefly, purified reconstituted ABC^{B1} (1.5–3 μg) was incubated with at least a 100-fold molar excess of probe to ensure completion of the reaction and to prevent ligand depletion. Reaction with each maleimide probe was undertaken with ABC^{B1} in the basal, AMP-PNP bound (prehydrolytic), and vanadate trapped (posthydrolytic) conformations to assess conformational changes during the catalytic cycle of the transporter (*42*). In order to quantify the extent of labeling with maleimide probe, each isoform was compared to the highly reactive 324C protein. The latter contains a cysteine residue introduced into a highly accessible extracellular loop in the protein. The extent of labeling was assessed by fluorographic densitometry following SDS−PAGE using the BioDocIt gel imaging system containing an UV light source. Labeling intensity (L) was plotted as a function of time and the maximum extent (L_{max}) and half-life ($t_{½}$) for the reaction determined by nonlinear regression of the exponential association curve: $L = L_{max} \cdot (1 - e^{-kt})$, where k is the association rate constant ($t_{½} = \ln 2/k$).

To assess the effects of covalent modification on function, the TM6 mutant isoforms were labeled to near completion with coumarin−maleimide prior to functional assessment of ATPase activity. The individual half-lives were used to approximate the time required to reach 90% labeling efficiency with coumarin−maleimide. Following labeling, the reconstituted samples were separated from the unbound probe by ultracentrifugation (100,000g, 20 min, 4 °C).

Photoaffinity Labeling of Mutant ABC^{B1} Isoforms: Effect of Covalent Modification by CM. Drug binding to purified, reconstituted ABC^{B1} was assessed by measuring the displacement of the photoactive modulator [^{125}I]-iodoarylazidoprazosin ([^{125}I]-IAAP). Proteoliposomes (0.25 μg) were incubated with 10 nM [^{125}I]-IAAP in the presence of nicardipine (30 μM) or vinblastine (100 μM) in a total volume of 30 μL for 2 h at 21 °C under subdued light. The samples were cooled for 10 min on ice and UV irradiated (100W, 5 cm, $\lambda = 265$ nm) for 7 min. Laemmli sample buffer (5×) was added and protein resolved by SDS−PAGE. The amount of [^{125}I]-IAAP bound to ABC^{B1} was determined by densitometry of autoradiograms. All values were expressed as a ratio of the amount bound in the absence of drug.

Modeling ABC^{B1} Single Cysteine Isoforms. The palmitoyloleoyl-phosphatidyl-ethanolamine embedded closed-state and semiopen state homology models of ABC^{B1} developed by O'Mara and Tieleman (*46*) were used in this analysis and represent the nucleotide-free state (semiopen model) and the ATP bound state (closed model), respectively (*46*). Although the semiopen model was constructed using elements of both MalK and Sav1866, it has been shown that the NBD:ICL interface (which was constrained during the modeling process (*46*)) is at least partially preserved during the transition from nucleotide free to nucleotide bound sates of P-gp (*47*). The effects of the experimental single cysteine point mutations were examined by computationally mutating the corresponding residues of the two ABC^{B1} homology models in SPDBViewer, prior to energy minimization (*48*).

Data Analysis. Nonlinear least-squares regression analysis was undertaken using the GraphPad Prism4 program. Three independent sample points were considered the minimum data set for analyses. The means of two samples were compared with a Student's t-test, whereas multiple sample comparisons with a control were done with ANOVA using a Dunnett's posthoc test. A P-value <0.05 was considered statistically significant.

RESULTS

Purified ABC^{B1} Isoforms. The purified, reconstituted ABC^{B1} isoforms containing a single cysteine residue in the cytoplasmic half-of TM6 ($TM6_{CYT}$) and its predicted cytosolic extension were all purified to approximately 90% with similar yields in the range 0.5–1.0 mg protein per liter of cultured High-5 cells. The cysteine-less isoform of ABC^{B1} (*24*), which is used as the reference protein for subsequent topographical investigations exhibited a basal V_{max} of 0.48 ± 0.10 μmol/min/mg ($K_M = 0.54 \pm 0.05$ mM). This activity was stimulated 2.85-fold by the modulator nicardipine to a V_{max} of 1.37 ± 0.19 μmol/min/mg, with no significant change in the affinity constant for ATP ($K_M = 0.38 \pm 0.03$ mM). Cysteine-less ABC^{B1} is functionally identical to the wild-type protein and justifies its use as a reference point to assess the effects of TM6 mutations (*24*). The effects of introducing a single cysteine at positions in the $TM6_{CYT}$ have been fully detailed in a previous paper (*44*), and none of the introductions abrogates the ability of ABC^{B1} to perform drug stimulated ATP hydrolysis. These studies have additionally demonstrated that none of the ABC^{B1} single cysteine mutations in TM6 confers impaired drug binding, suggesting that the residues mutated do not make a significant contribution to the initial drug–protein interaction (*44*). However, there was some evidence (i.e., altered potency and degree of ATPase stimulation by drugs) that the TMD:NBD communication was perturbed in some of the $TM6_{CYT}$ mutations.

Use of a Chemical Labeling to Probe Local Environment and Conformational Changes in the Intracellular Half and Cytoplasmic Extension of TM6. The focus of our present investigation was to extend previous studies (*24*) and to describe the topography of $TM6_{CYT}$ and how it changes as the protein progresses through the catalytic cycle. Three distinct states of the catalytic cycle were examined for accessibility to covalent labeling with CM (hydrophobic probe), FM (hydrophilic probe), and BM (zwitterionic probe). The cysteine-less isoform was again used as a control for nonspecific probe interaction, and we observed negligible labeling for FM, marginal labeling with BM, and a significant nonspecific association with CM (presumably driven by the hydrophobicity of this molecule). For each isoform, we determined the accessibility of each probe in the absence of drugs ("basal conformation"), as well as in the AMP-PNP bound state (representative of the prehydrolytic conformation) and in the presence of ADP−Vi (post hydrolytic state), which are known to be structurally distinct in ABC^{B1} (*26, 27*). Figure 1a shows a representative example for the efficiency of labeling V345C with CM in the basal conformation. The positive control lane refers to labeling of the G324C isoform for 300 min and was assigned a value of 100%. The data were quantified by densitometry and expressed graphically in Figure 1b. V345C was labeled fully ($L_{ext} = 112\%$) with a half-life for the reaction of $t_{½} = 47$ min. In contrast,

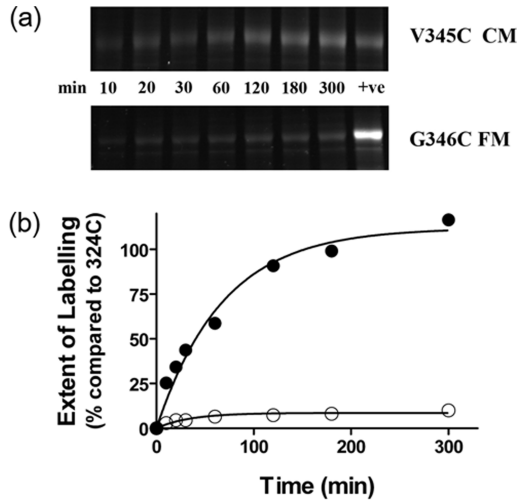

FIGURE 1: Labeling of single cysteine isoforms of ABC^{B1} by maleimides. (a) The V345C (upper gel) and G346C (lower gel) isoforms were reacted with CM and FM, respectively, for 10–300 min as described in Materials and Methods. The proteins were resolved using 8% SDS−PAGE and proteins visualized with the BioDocIt system using an UV light source. The "+ve" lane refers to labeling of the G324C isoform for 300 min (b) The SDS−PAGE data was quantified using densitometric analysis, and the values were expressed as a percentage of that obtained for the G324C isoform. The densities were plotted as a function of time and fitted with the hyperbolic association curve using nonlinear least-squares regression. Filled circles represent the labeling of V345C with CM, open circles represent the labeling of G346C with FM.

labeling of G346C with FM did not reach a significant extent ($L_{ext} = 7\%$), even after a 300 min incubation (Figure 1a,b).

A complete graphical representation of similar labeling time-courses of two selected isoforms (V345C and A354C) is shown in Figure 2. Under basal conditions, FM was unable to label residue 345C ($L_{ext} = 5 \pm 5\%$) to an extent that was significantly different to that observed in the cysteine-less protein. In contrast, the V345C isoform was highly accessible to CM, with complete labeling ($L_{ext} = 111 \pm 19\%$ $P < 0.05$) observed during the course of the reaction and partially accessible to the zwitterionic BM probe ($L_{ext} = 48 \pm 6\%$). Isoform V345C remained nonamenable to labeling with the hydrophilic FM when converted to the nucleotide bound or vanadate trapped conformation. Trapping V345C in these two conformations also failed to impact significantly on the extent of labeling observed under basal conditions for either BM or CM (Figure 2). This indicates that this residue neither changes its accessibility nor does it sense a change in the polarity of the local environment during the conformational changes ABC^{B1} undergoes during its catalytic cycle.

By contrast, isoform A354C (Figure 2) displays conformation dependent labeling of probes. This isoform displayed a low accessibility of labeling to FM ($L_{ext} = 34 \pm 1\%$) in the basal state. The addition of AMP-PNP caused a significant increase in the extent of labeling ($L_{ext} = 69 \pm 1\%$), and this was reduced to a level indistinguishable from that observed in the basal state for the vanadate trapped intermediate ($L_{ext} = 25 \pm 2\%$). Labeling with the hydrophobic CM probe was complete in the basal state ($L_{ext} = 82 \pm 7\%$) and unaffected by progression between the three catalytic intermediates of ABC^{B1}. BM labeled the A354C isoform equally well in the basal ($L_{ext} = 99 \pm 15\%$) and nucleotide bound conformations ($L_{ext} = 130 \pm 11\%$). However, progression from the nucleotide bound to the posthydrolytic (vanadate trapped)

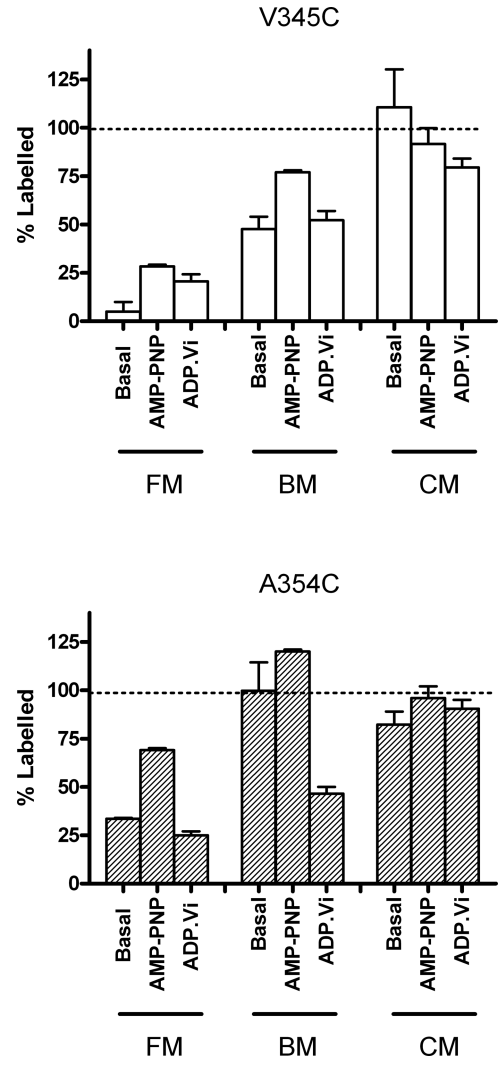

FIGURE 2: Accessibility of single cysteine ABC^{B1} isoforms to maleimide probes: effects of AMP-PNP and vanadate trapping. The maximal extent of labeling (L_{ext}) was ascertained for the (a) V345C and (b) A354C mutant isoforms of ABC^{B1} using the three maleimide containing probes, FM, BM and CM. The values of L_{ext} were obtained for proteins in the basal, AMP-PNP bound and vanadate trapped conformations of the proteins as described in Materials and Methods. The values represent the mean ± SEM obtained from at least three independent observations.

conformation produced a significant reduction in accessibility to BM ($L_{ext} = 47 \pm 3\%$, $P < 0.05$). The 354 position in ABC^{B1} displays considerable accessibility to maleimide probes, and this residue is subject to spatial reorganization during the progression of the protein through the catalytic cycle; in particular, for the labeling by BM posthydrolysis.

Similar analysis was undertaken for all the other ABC^{B1} isoforms containing mutations within TM6 in each transition conformation. The results are summarized in Table 1, which provides a qualitative assessment of the relative accessibility of the residues to covalent modification. The results are presented as (i) complete labeling during the reaction period (denoted +++), (ii) incomplete, but significantly different from the cysteine-less protein (denoted as + or ++ to enable easier identification of alterations in accessibility between conformational states), or (iii) unlabeled during the reaction (denoted −). Two striking features are evident from an examination of the data presented in the table, namely, a "polarity" of accessibility along the stretch from S344C

Table 1: Summary of Relative Accessibilities of TM6 Residues[a]

ABC^{B1} isoform	catalytic intermediate	FM	BM	CM
S344C	basal	−	+++	+++
	AMPPNP	+	+++	+++
	vanadate	+	+++	+++
V345C	basal	−	+	+++
	AMPPNP	+	++	+++
	vanadate	+	+	+++
G346C	basal	−	+	++
	AMPPNP	−	++	++
	vanadate	+	+	++
Q347C	basal	+	+	+++
	AMPPNP	+	+	++
	vanadate	+	+	+++
S349C	basal	−	+	+
	AMPPNP	+	++	+
	vanadate	−	++	+++
A354C	basal	+	+++	+++
	AMPPNP	++	+++	+++
	vanadate	+	+	+++
G360C	basal	+++	+++	++
	AMPPNP	+++	+++	++
	vanadate	+	++	+++

[a] The accessibility of each introduced cysteine residue was determined using fluorescein-maleimide (FM), BODIPY-maleimide (BM) or coumarin-maleimide (CM). The accessibility of labeling was compared to the cysteine-less isoform of ABC^{B1}. Complete labeling during the time-course of the experiment was denoted as (+++), whilst incomplete labeling was denoted with either (++) or (+) to enable clear illustration of changes in accessibility. No significant labeling of an isoform with a particular probe is denoted (−).

through to G360C and a disparity in the conformation dependent changes in accessibility.

First, residues at the apex of the labeled region (344 to 347) are in a hydrophobic environment, extensively labeled by the hydrophobic CM probe, partially labeled by the zwitterionic probe, and poorly labeled by the hydrophilic probe (FM). In the adjacent helical turn, residue 349 displays a reduction in CM labeling. Residues 354 and 360 show almost total labeling by BM (and CM, as are all residues) and extensive labeling by FM, demonstrating that these amino acids are in a more hydrophilic environment.

Second, the data show that residues at the N-terminus of our mutated region undergo little change in their accessibility during the catalytic cycle. There are only limited changes in accessibility to BM and FM displayed by residues 344–347 (Table 3), but these are minor in comparison with the changes in accessibility of the residues in the cytoplasmic extension of TM6. For instance, residue 360C shows an almost complete loss of labeled region with FM in the posthydrolytic state, a marked reduction in BM labeling, and a parallel increase in CM labeling. Similarly, large changes in accessibility are observed with A354C (Figure 2).

Coumarin−Maleimide Labeling of Single Cysteine Containing ABC^{B1} Isoforms Affects Drug Stimulated ATPase Activity. In the second phase of investigation, the functional consequences of perturbing TM6$_{CYT}$ topography were assessed. Topographical perturbation was achieved through covalent attachment of CM to the introduced cysteines, using time courses similar to those presented in Figure 1. CM was chosen since it labels each of the chosen residues, with the exception of S349C (data not shown). Functional characterization of the covalently modified isoforms was determined by measuring basal and drug stimulated ATPase activities.

The ATPase activity of the mutant isoforms is shown in Table 2, in the presence or the absence of covalent modification by CM. The data in Table 2 confirms previous findings (*44*) that the G346C and Q347C mutations provided the greatest impairment to ABC^{B1} activity with the underlying defect caused by impaired basal activity. None of the other mutations produced a significant alteration on the Michaelis–Menten kinetics or drug stimulation of ATP hydrolysis.

Table 2: Effects of Covalent Modification by CM on ATPase Activity of Mutant ABC^{B1} TM6 Isoforms[a]

	basal V_{max} (nmol P_i min^{-1} mg^{-1})			stimulated V_{max} (nmol P_i min^{-1} mg^{-1})		
	(−)CM	(+) CM	% change	(−)CM	(+) CM	% change
S344C	188 ± 62	192 ± 56		857 ± 216	317 ± 93*	−63
V345C	563 ± 85	388 ± 41	−31	1173 ± 355	937 ± 292	−20
G346C	101 ± 18	102 ± 12		268 ± 47	186 ± 59	−30
Q347C	66 ± 6	41 ± 15	−37	161 ± 33	61 ± 4*	−62
A354C	126 ± 10	229 ± 27*	+81	535 ± 72	353 ± 18*	−34
G360C	396 ± 82	508 ± 134	+28	1244 ± 252	810 ± 108	−34

[a] The ABC^{B1} isoforms containing mutations within TM6 were examined for ATPase activity prior to and following reaction with the hydrophobic maleimide probe CM. The isoforms were reacted with CM to ensure at least 90% modification. Michaelis−Menten analysis was undertaken in the presence or absence of 30 μM nicardipine to determine the maximal ATPase activity (V_{max}). Parameters were obtained by non-linear least squares regression, and the data represent the mean ± SEM of at least three independent observations. (*), indicates a statistically significant difference (ANOVA) compared to the value obtained in the absence of covalent modification by CM.

Table 3: Effects of Coumarin Labeling on the Potency of Drugs to Stimulate ATP Hydrolysis by Mutant ABC^{B1} TM6 Isoforms[a]

	EC_{50} nicardipine (μM)		EC_{50} vinblastine (μM)	
	(−) CM	(+) CM	(−) CM	(+) CM
S344C	3.0 ± 0.4	0.5 ± 0.1*	12.1 ± 0.5	na
V345C	2.3 ± 0.4	3.9 ± 0.6	4.9 ± 1.4	8.5 ± 1.9
G346C	4.8 ± 1.8	7.1 ± 1.7	na	na
Q347C	2.7 ± 0.4	1.9 ± 0.8	na	na
A354C	2.4 ± 0.2	1.6 ± 0.2	2.5 ± 0.2	na
G360C	2.7 ± 0.4	5.1 ± 0.2*	5.7 ± 0.1	8.6 ± 1.2

[a] The potency of nicardipine and vinblastine to stimulate ATP hydrolysis was examined for a wide range of drug concentrations (10^{-9}–10^{-4} M). The EC_{50} values for drug stimulation were obtained by non-linear least squares regression of the general dose−response equation. The data represent the mean ± SEM of at least three independent observations. (*), indicates a statistically significant difference (ANOVA) compared to the value obtained in the absence of covalent modification by CM.

The covalent modification of introduced cysteine residues produced effects in a number of the residues. While there were no effects on the basal ATPase activity for any of the mutant isoforms, except for a 2-fold increase in the basal ATPase activity of A354C following CM labeling (Table 2), there were numerous distinct effects on the maximal extent of drug stimulated ATPase activity. In addition, Table 3 shows that potencies of nicardipine and vinblastine to stimulate ATP hydrolysis were also modified by covalent attachment of CM to residues within TM6$_{CYT}$. Representative full dose–response data is shown for two isoforms (S344C and V345C) in Figure 3. S344C displayed a significant reduction in the V_{max} and degree of stimulation of ATP hydrolysis following the attachment of the coumarin moiety. As highlighted in Figure 3, the degree of stimulation by nicardipine was reduced from 4.8 ± 0.6-fold to 1.6 ± 0.1-fold by reaction with CM, albeit with a small increase in potency of the drug (Figure 3a). A more dramatic effect was observed in this isoform following CM modification, namely, that vinblastine could no longer stimulate the basal ATPase

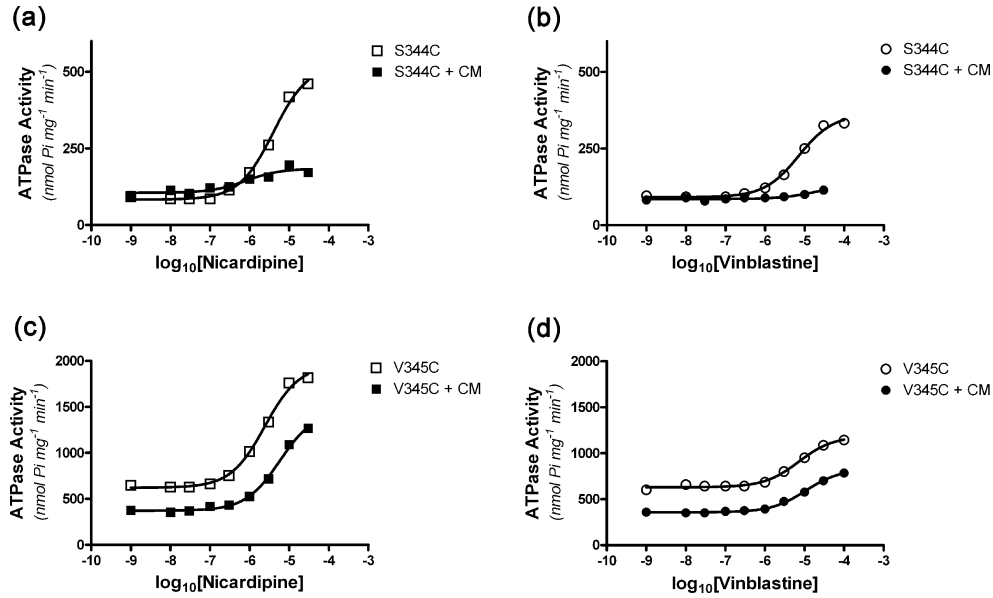

FIGURE 3: Effects of covalent attachment of CM on ATPase activity of mutant ABC^{B1} isoforms. ATPase activity was obtained for the S344C (a and b) and V345C isoforms (c and d) of ABC^{B1} prior to (empty symbols) or following the reaction with CM (filled symbols). The ATPase activity was ascertained in varying concentrations of either the modulator nicardipine (a and c) or the substrate vinblastine (b and d). The potencies and extents of stimulation of ATP hydrolysis were estimated following nonlinear least-squares regression of the general dose−response equation. Data in the figure was taken from a single representative example.

Table 4: Effects of Coumarin Labeling on Drug Binding in Mutant ABC^{B1} TM6 Isoforms[a]

	vinblastine			nicardipine		
	S344C	Q347C	A354C	S344C	Q347C	A354C
(−) CM	0.34 ± 0.09	0.39 ± 0.06	0.61 ± 0.11	0.35 ± 0.02	0.40 ± 0.03	0.64 ± 0.09
(+) CM	0.46 ± 0.06	0.34 ± 0.09	0.39 ± 0.21	0.27 ± 0.03	0.41 ± 0.06	0.57 ± 0.16

[a] [^{125}I]-IAAP photoaffinity labeling was undertaken in the S344C, Q347C and A354C mutant TM6 isoforms prior to and following labeling with coumarin maleimide. The amount of labeling was determined by densitometry of autoradiograms following SDS−PAGE as described in Materials and Methods. The intensity of [^{125}I]-IAAP labeling in the absence of drugs was assigned a value of 1.0. Values represent the mean ± SEM of the amount of [^{125}I]-IAAP bound in the presence of the displacing drugs nicardipine (30 μM) or vinblastine (100 μM). The values were obtained from four independent preparations of purified protein.

activity of the protein (Figure 3b). Clearly, this perturbation impairs the ability of drugs to induce the stimulation of ATP hydrolysis; moreover, it does so in a drug specific manner.

Covalent modification also impacted the ATPase activity of isoform V345C, albeit in a markedly distinct fashion to that observed with S344C (Table 2 and Figure 3c and d). The basal and nicardipine stimulated V_{max} values for ATP hydrolysis by CM modified V345C were indistinguishable from that observed with untreated protein (Table 2). Similarly, the degree of stimulation produced by nicardipine was unaffected by the covalent modification. Closer inspection of the drug−ABC^{B1} interaction revealed that covalent attachment of coumarin did in fact impact ATPase activity (Figure 3c and d). The nature of the effect was a significant ($P < 0.05$) reduction in the potency of both nicardipine and vinblastine to stimulate nucleotide hydrolysis (Table 3).

While the G346C isoform was unaffected by the reaction with CM, the V_{max} for nicardipine stimulated ATP hydrolysis was reduced 2-fold in the Q347C isoform (Table 2). A354C, which was avidly labeled by CM, displayed a both small reduction in the V_{max} for nicardipine stimulation of ATPase activity due to a reduced degree of stimulation by this compound. In fact, the low degree of stimulation rendered the assignment of potency for the stimulation of ATP hydrolysis problematic. G360C was less amenable to labeling with CM and only displayed a minor reduction in the potency of nicardipine to stimulate hydrolysis. Overall, the covalent attachment of CM to cysteine residues along the cytosolic half of TM6 generated a number of drug specific effects on ATP hydrolysis. The main manifestations were a reduction in the degree of stimulation or the potency characteristic of the stimulation.

Drug Binding To TM6 Mutant Isoforms: Effects of Coumarin Maleimide Labeling. We have previously demonstrated that mutation of residues within TM6$_{CYT}$ does not affect the binding of the modulator [^{125}I]-IAAP. The isoforms S344C, Q347C, and A354C displayed significant reductions in drug stimulated ATP hydrolysis following CM labeling, and this may be attributed to altered drug binding. Consequently, the ability of nicardipine and vinblastine to displace [^{125}I]-IAAP labeling was examined in these isoforms in the presence or absence of CM labeling. The fraction of [^{125}I]-IAAP displaced by the two drugs in the control and labeled protein is shown in Table 4. There was no measurable effect of CM labeling on the ability of either nicardipine or vinblastine to displace [^{125}I]-IAAP from the proteins. This suggests that the initial binding interaction between the two drugs is not adversely disrupted by labeling with CM.

DISCUSSION

A great deal of accumulated evidence indicates a pivotal role for TM6 in the drug translocation process by ABC^{B1},

and elucidating mechanistic details of this role was the focus of the present investigation. Our modus operandi involves introducing unique cysteine residues along the cytosolic half of TM6 and the subsequent covalent attachment of coumarin−maleimide to these. Recent data on bacterial light harvesting complexes has demonstrated that the TM helices are remarkably robust to mutations that drastically alter the size of a given residue, thus supporting the idea that site-directed mutants of membrane proteins can act as valid reporters of function, rather than being dismissed as structurally disruptive (*49*). Following labeling, three of the residues we have studied (S344C, Q347C, and A354C) were associated with a reduction in the magnitude to which drug substrates stimulate ATP hydrolysis. In addition, an alteration in the potency of the stimulation, or abrogation of ATPase activity, was observed for a number of residues (S344C, V345C, S349C, A354C, and G360C). What is the mechanism underlying the effect of covalent modification of TM6 on the coupling of drug binding in the TMD to ATP hydrolysis by the NBDs? There are two likely possibilities: (a) impaired drug binding to TM6 or nearby helices or (b) perturbation of communication pathways between TM6 and the NBDs.

Numerous attempts have been made during the last two decades to elucidate the location of drug binding sites in ABC^{B1} and several focused on TM6 (*29–36*). A number of the helices within the TMDs have been implicated in mediating drug binding, and a clear picture has not yet been obtained. Investigations using a cysteine-scanning mutagenesis approach suggest a single domain or "bowl" that comprises TMs 1, 4–6, and 10–12 (*29–36, 50*). Recently, TM7 has also been added to the list of helices contributing to drug binding (*50*). The strategy used to identify a binding "bowl" involved the use of the cysteine reactive "substrate" MTS-verapamil. Labeling of residues could therefore be attributed to either interaction at the true pharmacophoric region, or alternatively, the covalent attachment of the methane−thiosulfonate moiety to accessible cysteine residues. In contrast, the combination of photoaffinity drug labeling and mass spectroscopic analysis (MALDI-TOF) has identified a different potential region for drug interaction on ABC^{B1} (*36, 51*). These elegant studies define the interfacial region of TM segments 3/11 and 5/8 as the binding site for the propafenone class of ABC^{B1} substrates. Further evidence arguing against a role of TM6 in drug binding has been obtained using photoaffinity labeling of ABC^{B1} isoforms containing single cysteine residues introduced throughout TM6 (*42, 44*). In particular, the binding of a 1,4-dihydropyridine ([^{3}H]-azidopine) and a prazosin analogue ([^{125}I]-IAAP) did not directly involve TM6 (*42, 44*). Moreover, in the present article, we have demonstrated that binding of nicardipine and vinblastine were unaffected by labeling several TM6 isoforms with CM. Therefore, we believe that the perturbation of drug stimulated ATP hydrolysis caused by covalent attachment of CM to TM6 is most likely due to the modification of the communication pathway that links the drug-binding event in the TMD to the progression of the catalytic cycle in the NBDs. The communication pathway clearly involves TM6, given that mutations or covalent modification within this helix impairs drug stimulated ATPase activity (*42, 44*). We acknowledge that the differences in the literature regarding the role of TM6 in drug binding or subsequent events is unlikely to be resolved by methods that rely on covalent interactions of drug (or drug analogue) with protein. The true nature of the drug−protein interaction is a reversible noncovalent interaction, and only classical pharmacological studies of mutant P-gp isoforms with nonmodified drug substrates may reveal the role of residues in drug binding.

What is the nature of involvement of TM6 in the TMD ↔ NBD communication pathway? To address this question, the topography of the cytosolic half-of TM6 was examined in distinct conformations of ABC^{B1}. The conformations reflected the progression of the protein through the catalytic cycle and was visualized by the accessibility of engineered cysteines to covalent modification by maleimide probes. The observations were also undertaken for two residues (A354C and G360C) within the extension of TM6 that links the helix to the N-terminal NBD. This cytosolic extension was highly accessible to covalent modification, regardless of the physicochemical properties of the different probes. In addition, the extension displayed different accessibility to probes when the protein was trapped in distinct conformations (e.g., posthydrolysis), thereby reflecting conformational transitions. The region including V345C and S349C was relatively intransigent to covalent modification with either FM or BM. Moreover, this region of TM6 did not display altered accessibility to maleimide probes as the protein was processed through the basal, ATP-bound, and vanadate trapped configurations. This lack of change is in contrast to the considerable conformational changes previously observed in the segment between V331C to F343C (*42*). Residue S344C, which is located in the central region of TM6, was considerably more accessible to covalent modification than the more cytosolic region of the helix. This is in good agreement with the data from Rothnie et al. demonstrating similar high accessibility for the adjacent residue, F343C (*42*). The residue at the proposed cytosolic terminus of TM6 (S349C) displayed the greatest propensity for changes in accessibility, indicating conformational flexibility in this region of the helix.

In the absence of a high resolution structure for P-glycoprotein, it is necessary to use homology models to assist in the interpretation of this data. Our objective molecular models of P-gp in the semiopen (basal) and closed (ATP/AMP-PNP bound) states (*46*) allow such an interpretation. Analysis of both of these models shows that V345 is at the closest point of contact among TM4, 5, and 6. V345 interacts sterically with Leu225 (TM4) and Ile306 (TM5) to form a tight triad, coordinating interhelix interactions (Figure 4a and b). Looser triple contact points among TM4, 5, and 6 were found at helical turns immediately above and below the V345/L225/I306 triad. It is well established that the mutual interactions of hydrophobic residues such as valine, isoleucine, and leucine in the interior of a protein are important for correct protein folding through knobs-into-holes interlacing of side chains (*52*) and that trimeric α-helical packing can be stabilized preferentially by β-branched amino residues (*53*). *In silico* mutation of the β-branched valine residue to a slightly smaller cysteine residue, while less favorable in terms of residue packing, did not have a significant impact on the interhelical interactions of the V345C/L225/I306 triad. The modeled side chain of V345C faces away from the pore in the basal state model, rendering it inaccessible to the hydrophilic FM probe and only partially accessible to the zwitterionic BM probe, in accordance with the data presented

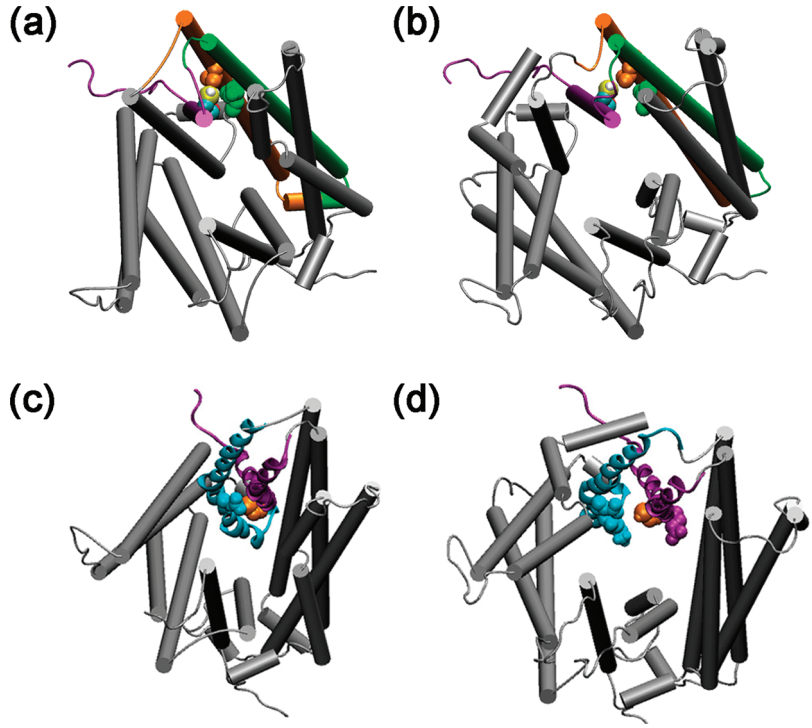

FIGURE 4: Molecular modeling insight into the V345C and A354C mutations in ABC^{B1}. The top view of the ABC^{B1} transmembrane domain, viewed from the extracellular side of the membrane. (a) In the AMP-PNP bound state, the V345C (spacefill, CPK coloring) is inaccessible to the translocation pore. Close interhelix contacts are shown for TM4 (orange), TM5 (green) and TM6 (purple). The closest point of contact between the helices is V345C, which interacts hydrophobically with Leu225 (orange) and Ile306 (green). (b) The modeled basal state shows only minor reorganizations of the V345C−L225−I306 triad, consistent with the experimental findings. (c) A view from the top of the pore shows the AMP-PNP configuration: A354C (orange) hydrogen bonds to its nearest neighbour, D188 (cyan). (d) In the basal state, conformational changes disrupt the TM3-TM6 coiled-coil motif and break the D188-V345C hydrogen bond. Adjacent charged residues from TM3 (cyan) and TM6 (purple) face the translocation pore, while A354C is situated in a cleft between TM3 and TM6.

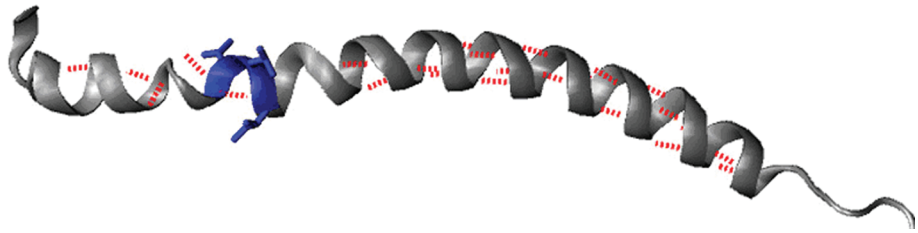

FIGURE 5: Disruption of helical hydrogen bonding pattern induced by three adjacent β-branched residues. TM6 is represented as a ribbon, with the TM5-6 linker shown on the left and the ICD connection to the NBD on the right. The bulky side chains of adjacent β-branched residues, V338-L339-I340 (shaded blue), destabilize the α-helical packing of TM6, indicated by the disruption of the hydrogen bonding pattern (red dashed lines) in the adjacent turns.

here (Figure 4a and Table 1). Analysis of the AMP-PNP state model (which exhibits a "nucleotide sandwich dimer") suggests that a set of coordinated rotational and tilt angle changes in TM4, 5, and 6 around the V345C/L225/I306 triad occurs without altering the exposure of residue 345 itself (Figure 4b). Interestingly, residue V345 is also proximal to S222 (TM4), which has been implicated in the binding of MTS-verapamil to P-gp (*33*). The side chain of S222 is somewhat more exposed in our closed-state model (representing the basal state, which has a high affinity for drugs (*28*)) than in the AMP-PNP bound state (which has a lower affinity for drugs (*28*)).

Similar analysis helps rationalize the A354C data and provides further evidence that our homology models are a valid reflection of TM helix packing. An examination of the ABC^{B1} models showed the proposed membrane-embedded region of TM6 packs against TM3 through an α-helical coiled-coil interaction (Figure 4c and d). A354C forms part of the TM3−TM6 contact interface with the sulfur atom being accessible to the translocation pore, thus enabling covalent modification by the hydrophilic FM and zwitterionic BM probes. Further examination of the residues adjacent to A354C revealed a number of charged and polar residues in its immediate vicinity, in particular, K181, E184, and D188 from TM3, and the adjacent E353 from TM6, creating a favorable local environment for FM and BM. Comparison of the AMP-PNP state model with the basal state model shows a disruption of the TM3−TM6 interface around A354C (Figure 4c). In the basal conformation homology model, the side chain of A354C was angled away from the pore, while charged residues in the local vicinity faced into the translocation pore (Figure 4d), decreasing the surface accessibility of A354C to the translocation pore and thus the accessibility to FM. The position of A354C at the interface of TM3 and TM6, which both have a lipid exposed face, allowed the hydrophobic CM probe to access A354C through the bilayer.

On the basis of the observations in the present investigation and from previous studies (*42–44*), it appears that TM6

undergoes distinct changes in conformation in response to events occurring in the NBDs. The greatest degree of conformational alteration occurs at the two "ends" of the helix and in particular at the cytosolic extension, proximal to the NBD. Our model predicts that TM6 contains a central destabilization (Figure 5) due to the presence of three adjoining bulky hydrophobic residues V338/L339/I340, which disrupt helical packing. Disruption of L339 has been demonstrated to confer impaired ATPase activity, and the residue has been identified as being involved in energetic coupling by ABC^{B1} (*43*). The residues 338–340 are capped by S337 and G341, thereby generating a GxxxG-like motif. The GxxxG motif has been implicated in the packing and or dimerization of transmembrane helices by acting as a "ridge−groove" structure (*54, 55*). By acting in a similar manner in ABC^{B1}, the region S337-G341 could facilitate the packing of TM6 to neighboring helices and thereby permit transduction of binding events in the protein. Notably, the GxxxG motif is conserved in TM12 as well (residues 980–984 AVVFG) and in ABC^{B1} from other mammals, and we investigated whether the equivalent residues in TM12 adopt a similar functional significance. Alternatively, the motif may act as a central pivot in the helix about which the ends of the helices and the cytosolic extension can move. This could also facilitate the transmission of conformational changes in neighboring helices to the NBDs using TM6 as a conduit. This is in agreement with the key role for TM6 in mediating the stimulation of ATP hydrolysis by numerous drugs that interact at pharmacologically distinct sites in ABC^{B1}.

REFERENCES

1. Modok, S., Mellor, H. R., and Callaghan, R. (2006) Modulation of multidrug resistance efflux pump activity to overcome chemoresistance in cancer. *Curr. Opin. Pharmacol. 6*, 350–354.
2. Gottesman, M. M., Fojo, T., and Bates, S. E. (2002) Multidrug resistance in cancer: role of ATP-dependent transporters. *Nat. Rev. Cancer 2*, 48–58.
3. Leonard, G. D., Fojo, T., and Bates, S. E. (2003) The role of ABC transporters in clinical practice. *Oncologist 8*, 411–424.
4. Wang, R. B., Kuo, C. L., Lien, L. L., and Lien, E. J. (2003) Structure-activity relationship: analyses of p-glycoprotein substrates and inhibitors. *J. Clin. Pharm. Ther. 28*, 203–228.
5. Clark, R., Kerr, I. D., and Callaghan, R. (2006) Multiple drug-binding sites on the R482G isoform of the ABCG2 transporter. *Br. J. Pharmacol. 149*, 506–515.
6. Martin, C., Berridge, G., Higgins, C. F., Mistry, P., Charlton, P., and Callaghan, R. (2000) Communication between multiple drug binding sites on P-glycoprotein. *Mol. Pharmacol. 58*, 624–632.
7. Rothnie, A., Callaghan, R., Deeley, R. G., and Cole, S. P. (2006) Role of GSH in estrone sulfate binding and translocation by the multidrug resistance protein 1 (MRP1/ABCC1). *J. Biol. Chem. 281*, 13906–13914.
8. Ayesh, S., Shao, Y.-M., and Stein, W. D. (1996) Co-operative, competitive and non-competitive interactions between modulators of P-glycoprotein. *Biochim. Biophys. Acta 1316*, 8–18.
9. Ferry, D. R., Russell, M. A., and Cullen, M. H. (1992) P-glycoprotein possesses a 1,4-dihydropyridine selective drug acceptor site which is allosterically coupled to a vinca alkaloid selective binding site. *Biochem. Biophys. Res. Commun. 188*, 440–445.
10. Pascaud, C., Garrigos, M., and Orlowski, S. (1998) Multidrug resistance transporter P-glycoprotein has distinct but interacting binding sites for cytotoxic drugs and reversing agents. *Biochem. J. 333*, 351–358.
11. Shapiro, A. B., and Ling, V. (1997) Positively cooperative sites for drug transport by P-glycoprotein with distinct drug specificities. *Eur. J. Biochem. 250*, 130–137.
12. al-Shawi, M. K., and Senior, A. E. (1993) Characterization of the adenosine triphosphatase activity of Chinese hamster P-glycoprotein. *J. Biol. Chem. 268*, 4197–4206.
13. al-Shawi, M. K., Urbatsch, I. L., and Senior, A. E. (1994) Covalent inhibitors of P-glycoprotein ATPase activity. *J. Biol. Chem. 269*, 8986–8992.
14. Loo, T. W., and Clarke, D. M. (1994) Reconstitution of drug-stimulated ATPase activity following co- expression of each half of human P-glycoprotein as separate polypeptides. *J. Biol. Chem. 269*, 7750–7755.
15. Urbatsch, I. L., Sankaran, B., Bhagat, S., and Senior, A. E. (1995) Both P-glycoprotein nucleotide-binding sites are catalytically active. *J. Biol. Chem. 270*, 26956–26961.
16. Ambudkar, S. V., Cardarelli, C. O., Pashinsky, I., and Stein, W. D. (1997) Relation between the turnover number for vinblastine transport and for vinblastine-stimulated ATP hydrolysis by human P-glycoprotein. *J. Biol. Chem. 272*, 21160–21166.
17. Delannoy, S., Urbatsch, I. L., Tombline, G., Senior, A. E., and Vogel, P. D. (2005) Nucleotide binding to the multidrug resistance P-glycoprotein as studied by ESR spectroscopy. *Biochemistry 44*, 14010–14019.
18. Eytan, G. D., Regev, R., and Assaraf, Y. G. (1996) Functional reconstitution of P-glycoprotein reveals an apparent near stoichiometric drug transport to ATP hydrolysis. *J. Biol. Chem. 271*, 3172–3178.
19. Sauna, Z. E., and Ambudkar, S. V. (2000) Evidence for a requirement for ATP hydrolysis at two distinct steps during a single turnover of the catalytic cycle of human P-glycoprotein. *Proc. Natl. Acad. Sci. U.S.A. 97*, 2515–2520.
20. Shapiro, A. B., and Ling, V. (1995) Using purified P-glycoprotein to understand multidrug resistance. *J. Bioenerg. Biomembr. 27*, 7–13.
21. Tombline, G., Muharemagic, A., White, L. B., and Senior, A. E. (2005) Involvement of the "occluded nucleotide conformation" of p-glycoprotein in the catalytic pathway. *Biochemistry 44*, 12879–12886.
22. Loo, T. W., and Clarke, D. M. (1995) Membrane topology of a cysteine-less mutant of human P-glycoprotein. *J. Biol. Chem. 270*, 843–848.
23. Ramachandra, M., Ambudkar, S. V., Chen, D., Hrycyna, C. A., Dey, S., Gottesman, M. M., and Pastan, I. (1998) Human P-glycoprotein exhibits reduced affinity for substrates during a catalytic transition state. *Biochemistry 37*, 5010–5019.
24. Taylor, A. M., Storm, J., Soceneantu, L., Linton, K. J., Gabriel, M., Martin, C., Woodhouse, J., Blott, E., Higgins, C. F., and Callaghan, R. (2001) Detailed characterization of cysteine-less P-glycoprotein reveals subtle pharmacological differences in function from wild-type protein. *Br. J. Pharmacol. 134*, 1609–1618.
25. Rosenberg, M. F., Callaghan, R., Modok, S., Higgins, C. F., and Ford, R. C. (2005) Three-dimensional structure of P-glycoprotein: the transmembrane regions adopt an asymmetric configuration in the nucleotide-bound state. *J. Biol. Chem. 280*, 2857–2862.
26. Rosenberg, M. F., Kamis, A. B., Callaghan, R., Higgins, C. F., and Ford, R. C. (2003) Three-dimensional structures of the mammalian multidrug resistance P- glycoprotein demonstrate major conformational changes in the transmembrane domains upon nucleotide binding. *J. Biol. Chem. 278*, 8294–8299.
27. Rosenberg, M. F., Velarde, G., Ford, R. C., Martin, C., Berridge, G., Kerr, I. D., Callaghan, R., Schmidlin, A., Wooding, C., Linton, K. J., and Higgins, C. F. (2001) Repacking of the transmembrane domains of P-glycoprotein during the transport ATPase cycle. *EMBO J. 20*, 5615–5625.
28. Martin, C., Higgins, C. F., and Callaghan, R. (2001) The vinblastine binding site adopts high- and low-affinity conformations during a transport cycle of P-glycoprotein. *Biochemistry 40*, 15733–15742.
29. Bruggemann, E. P., Currier, S. J., Gottesman, M. M., and Pastan, I. (1992) Characterization of the azidopine and vinblastine binding site of P-glycoprotein. *J. Biol. Chem. 267*, 21020–21026.
30. Demeule, M., Laplante, A., Murphy, G. F., Wenger, R. M., and Beliveau, R. (1998) Identification of the cyclosporin-binding site in P-glycoprotein. *Biochemistry 37*, 18110–18118.
31. Greenberger, L. M. (1993) Major photoaffinity drug labeling sites for iodoaryl azidoprazosin in P-glycoprotein are within, or immediately C-terminal to, transmembrane domains 6 and 12. *J. Biol. Chem. 268*, 11417–11425.
32. Kwan, T., and Gros, P. (1998) Mutational analysis of the P-glycoprotein first intracellular loop and flanking transmembrane domains. *Biochemistry 37*, 3337–3350.
33. Loo, T. W., and Clarke, D. M. (2001) Defining the drug-binding site in the human multidrug resistance P-glycoprotein using a methanethiosulfonate analog of verapamil, MTS-verapamil. *J. Biol. Chem. 276*, 14972–14979.

34. Loo, T. W., and Clarke, D. M. (2002) Location of the rhodamine-binding site in the human multidrug resistance P-glycoprotein. *J. Biol. Chem. 277*, 44332–44338.
35. Maki, N., Moitra, K., Ghosh, P., and Dey, S. (2006) Allosteric modulation bypasses the requirement for ATP hydrolysis in regenerating low affinity transition state conformation of human P-glycoprotein. *J. Biol. Chem. 281*, 10769–10777.
36. Pleban, K., Kopp, S., Csaszar, E., Peer, M., Hrebicek, T., Rizzi, A., Ecker, G. F., and Chiba, P. (2005) P-glycoprotein substrate binding domains are located at the transmembrane domain/transmembrane domain interfaces: a combined photoaffinity labeling-protein homology modeling approach. *Mol. Pharmacol. 67*, 365–374.
37. Devine, S. E., Ling, V., and Melera, P. W. (1992) Amino acid substitutions in the sixth transmembrane domain of P- glycoprotein alter multidrug resistance. *Proc. Natl. Acad. Sci. U.S.A. 89*, 4564–4568.
38. Loo, T. W., and Clarke, D. M. (1994) Mutations to amino acids located in predicted transmembrane segment 6 (TM6) modulate the activity and substrate specificity of human P- glycoprotein. *Biochemistry 33*, 14049–14057.
39. Loo, T. W., and Clarke, D. M. (1996) Inhibition of oxidative cross-linking between engineered cysteine residues at positions 332 in predicted transmembrane segments (TM) 6 and 975 in predicted TM12 of human P-glycoprotein by drug substrates. *J. Biol. Chem. 271*, 27482–27487.
40. Ma, J. F., Grant, G., and Melera, P. W. (1997) Mutations in the sixth transmembrane domain of P-glycoprotein that alter the pattern of cross-resistance also alter sensitivity to cyclosporin A reversal. *Mol. Pharmacol. 51*, 922–930.
41. Song, J., and Melera, P. W. (2001) Further characterization of the sixth transmembrane domain of Pgp1 by site-directed mutagenesis. *Cancer Chemother. Pharmacol. 48*, 339–346.
42. Rothnie, A., Storm, J., Campbell, J., Linton, K. J., Kerr, I. D., and Callaghan, R. (2004) The topography of transmembrane segment six is altered during the catalytic cycle of P-glycoprotein. *J. Biol. Chem. 279*, 34913–34921.
43. Rothnie, A., Storm, J., McMahon, R., Taylor, A., Kerr, I. D., and Callaghan, R. (2005) The coupling mechanism of P-glycoprotein involves residue L339 in the sixth membrane spanning segment. *FEBS Lett. 579*, 3984–3990.
44. Storm, J., O'Mara, M. L., Crowley, E. H., Peall, J., Tieleman, D. P., Kerr, I. D., and Callaghan, R. (2007) Residue G346 in Transmembrane Segment Six is Involved in Inter-Domain Communication in P-Glycoprotein. *Biochemistry 46*, 9899–9910.
45. Chifflet, S., Chiesa, U. T. R., and Tolosa, S. (1988) A method for the determination of inorganic phosphate in the presence of labile organic phosphate and high concentrations of protein: application to lens ATPases. *Anal. Biochem. 168*, 1–4.
46. O'Mara, M. L., and Tieleman, D. P. (2007) P-glycoprotein models of the apo and ATP-bound states based on homology with Sav1866 and MalK. *FEBS Lett. 581*, 4217–4222.
47. Zolnerciks, J. K., Wooding, C., and Linton, K. J. (2007) Evidence for a Sav1866-like architecture for the human multidrug transporter P-glycoprotein. *FASEB J. 21*, 3937–3948.
48. Guex, N., and Peitsch, M. C. (1997) SWISS-MODEL and the Swiss-PdbViewer: an environment for comparative protein modeling. *Electrophoresis 18*, 2714–2723.
49. Fyfe, P. K., Potter, J. A., Cheng, J., Williams, C. M., Watson, A. J., and Jones, M. R. (2007) Structural responses to cavity-creating mutations in an integral membrane protein. *Biochemistry 46*, 10461–10472.
50. Loo, T. W., Bartlett, M. C., and Clarke, D. M. (2006) Transmembrane segment 7 of human P-glycoprotein forms part of the drug-binding pocket. *Biochem. J. 399*, 351–359.
51. Chiba, P., Mihalek, I., Ecker, G. F., Kopp, S., and Lichtarge, O. (2006) Role of transmembrane domain/transmembrane domain interfaces of P-glycoprotein (ABCB1) in solute transport. Convergent information from photoaffinity labeling, site directed mutagenesis and in silico importance prediction. *Curr. Med. Chem. 13*, 793–805.
52. Crick, F. (1953) The packing of [alpha]-helices: simple coiled-coils. *Acta Crystallogr. 6*, 689–697.
53. Harbury, P. B., Kim, P. S., and Alber, T. (1994) Crystal structure of an isoleucine-zipper trimer. *Nature 371*, 80–83.
54. Russ, W. P., and Engelman, D. M. (2000) The GxxxG motif: a framework for transmembrane helix-helix association. *J. Mol. Biol. 296*, 911–919.
55. Senes, A., Gerstein, M., and Engelman, D. M. (2000) Statistical analysis of amino acid patterns in transmembrane helices: the GxxxG motif occurs frequently and in association with beta-branched residues at neighboring positions. *J. Mol. Biol. 296*, 921–936.

BI7023089